ELSEVIER

Landscape and Urban Planning 34 (1996) 171–181

LANDSCAPE AND URBAN PLANNING

The effect of slopes on sand transport — numerical modelling

Haim Tsoar [a,*], Bruce White [b], Eugene Berman [c]

[a] *Department of Geography and Environmental Development, Ben-Gurion University of the Negev, Beer-Sheva 84105 , Israel*
[b] *Department of Mechanical and Aeronautical Engineering, University of California, Davis, CA 95616, USA*
[c] *CAD, CAM and CAE Laboratory, Ben-Gurion University of the Negev, Beer-Sheva 84105, Israel*

Abstract

Most aeolian sediment transport models and experiments have been conducted on flat horizontal surfaces. Very little numerical or analytical research has been carried out for aeolian sand transport on slopes. The current work presents numerical modelling of saltating sand for a climbing dune which has a slope angle of 20°. The model utilised wind fields predicted from the FAA complex terrain model for two dimensional escarpment and field data and wind-tunnel measurements for flow over a scaled model. Results suggest that only particles smaller than 0.230 mm are able to climb this slope under a wind shear velocity of 30 cm s^{-1}. The field observations and measurements confirm the numerical results.

Keywords: Slopes; Sand transport; Numerical modelling; Climbing dune

1. Introduction

In spite of the great advance made in understanding the physics of sand transport in saltation since the early works of (Bagnold, 1941) and (Chepil, 1945), all models proposed refer to the saltation process along a horizontal surface (Anderson, 1989). This also is true for wind-tunnel experiments that were carried out in horizontal test sections (Willetts and Rice, 1989).

The shear stress necessary to initiate the motion of a sand grain varies relative to the inclination of the surface. It is less easy to transport sand on an upslope than on flat or downsloping surfaces. Additionally, there are numerical flow models showing that wind over slopes displays important variations from airflow over a flat or undisturbed surface. Topographical obstacles give rise to perturbations in the flow, which in turn generate variations in shear stress (Taylor and Gent, 1974; Jackson and Hunt, 1975; Jensen and Zeman, 1985; Hunt et al., 1988a; Hunt et al., 1988b). Few, if any, have attempted to build a theoretical model which combines the vector of the forces exerted on grains by the wind on tilted surfaces with the variations in shear velocity and in turbulence characteristics ensuing from flow over slopes.

Most natural sand surfaces are not horizontal. Sand dunes have a convex shape with different aspect ratios of h/L (h is the height of the dune, and L is the characteristic dune horizontal width or length). Hence, most natural sand transport occurs on slopes with inclinations between zero and the angle of repose, which is about 33° for most sand-sized material. The recently developed statistical mathematical models of aeolian sand transport (Anderson et al., 1991) do not address inclined surfaces.

* Corresponding author.

SSDI 0169-2046(95)00235-9

The purpose of this work is to develop a numerical analysis that will develop into equations of aeolian sand transport on slopes. Field measurements taken on a climbing dune in the Negev desert of Israel, and wind-tunnel measurements on a model of the climbing dune provide validation of the FAA wind flow empirical model. The field climbing dune is about 20 m high and has a slope of about 20° (Figs. 1 and 2). The numerical and experimental works have a slope of the same dimension.

2. Field experiment: the effect of transport on slopes on sand texture

The texture of sand is a very sensitive factor that reflects changes in the transportation capacity and competence of the wind. Larger particles can be moved by very strong wind shear stress that may occur at the upper part of the slope. However, the effect of gravity on these grains, that depends on the weight of the grain and the slope ($mg \sin\theta$), will act against the strong shear stress of the wind.

It is conjectured that if it is harder to transport grains upslope, then only finer grains will be capable of climbing steep slopes, while on gentle slopes coarser grains can climb under identical dynamic conditions. Sand dunes display a great variety of shapes, profiles and grain sizes in a steady state. Low flat dunes (low h/L) display a coarse mean grain size, while steep dunes (higher h/L) are composed of fine mean grain size (Tsoar, 1986; Nielson and Kocurek, 1986). Also it is known that plinths of sand dunes are composed of coarse sand, while the upper slopes and crest are composed of much finer sand (Tsoar, 1990). There is no indication in the literature of the grain-size distribution along a climbing dune, which should reflect very clearly the effect of the slope on the sand movement.

Sand for grain-size distribution analysis was collected in the field from sand traps, similar to a trap developed by Leatherman (1978). The traps were deployed along the slope of the climbing dune (Fig. 2). Surface sand samples were retrieved from the face of the dune near the traps. The grain-size distribution analysis was done by means of standard sieves suspended on a shaker. The particle-size diameter was measured in the phi (ϕ) grade scale; where $2^{-\phi} = d$, where d is the grain-size in mm. Each sieve's aperture was greater by $1/4\phi$ than the one above it.

There is a considerable difference between the grain-size distribution of the sand traps (Fig. 3) and the surface samples' sand (Fig. 4). Dune sand gener-

Fig. 1. Photograph of the climbing dune in the Negev desert.

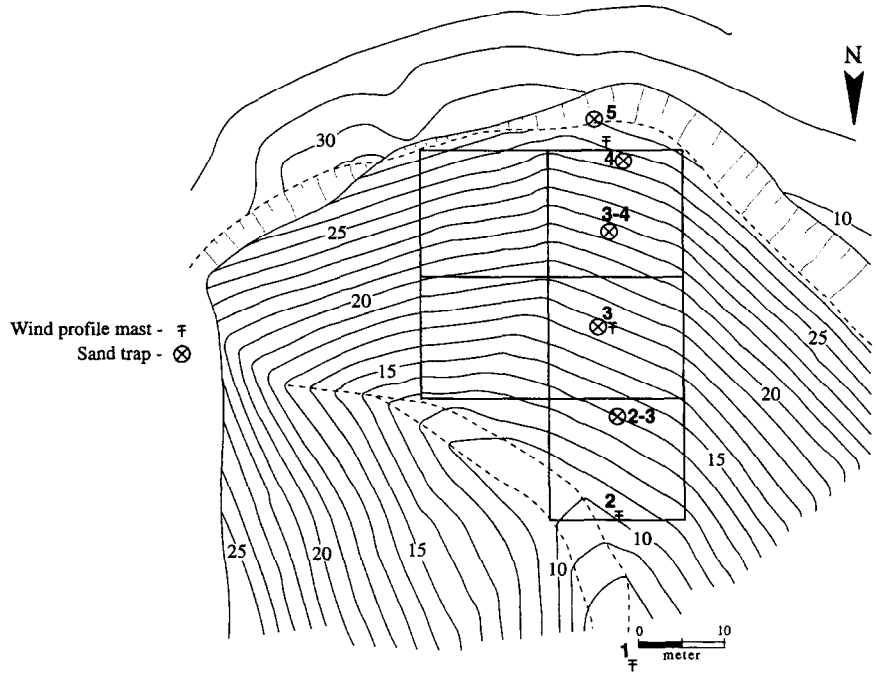

Fig. 2. Topographic map of the climbing dune shown in Fig. 1. Contour elevations are given in meters. The squares on the map link reference points marked in the field. The bold numbers indicate the location where sand samples were retrieved from the surface and from sand traps.

ally has a normal unimodal distribution in the fine sand range (0.125–0.250 mm; 3–2ϕ) (Ahlbrandt, 1979). All samples collected from the climbing dune showed a very clear bi-modal distribution with a coarse mode of 2.25ϕ and a fine mode of 2.75ϕ.

The results showed very clearly the difference between the two stages of erosion (trap sand) and deposition (surface sand). The surface sand was coarser than the trapped sand because the latter is only made of saltating sand while the coarser grains did not saltate but move mostly by rolling along the ground (surface creep) (Pye and Tsoar, 1990). The coarse mode of surface sand decreased gradually with the elevation of the climbing dune to such

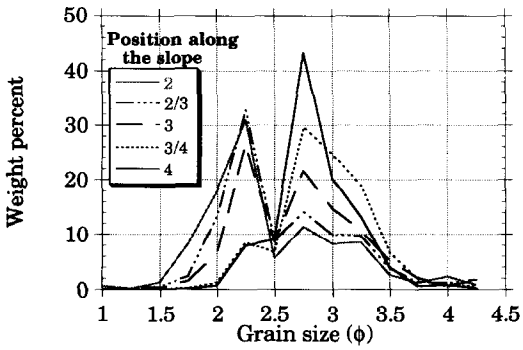

Fig. 3. Grain size distribution of sand samples retrieved from four traps (see Fig. 2) deployed on the climbing dune.

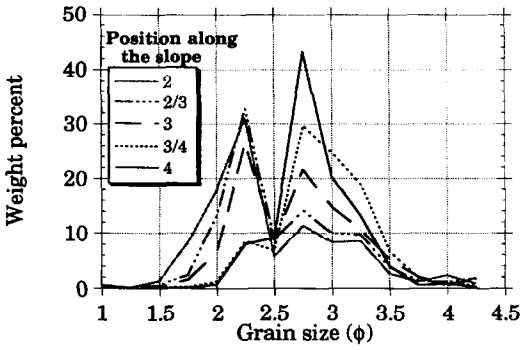

Fig. 4. Grain size distribution of sand samples from the surface of the climbing dune near the traps.

extent that, at Samples 3–4 and 4 (located at the upper portion of the climbing dune), it disappeared. Most of the sand on the surface at the plinth of the climbing dune (Samples 2 and 2–3) was between 1.5ϕ to 2.5ϕ (0.364–0.177 mm). Three important conclusions were drawn from the results:

1. There was a decrease in surface grain-size as the dune was climbed, which was indicated by the decrease in the coarse mode toward the crest.
2. The grains of the coarse mode were lag deposits that cannot be moved upslope by the wind shear stress. The effect of the slope was actually winnowing away the fine particles at lower elevations of the slope and leaving behind the coarse ones.
3. The most important change in grain size occurred between Sampling Points 3 and 3–4 where grains coarser than 2ϕ (0.26 mm) did not reach the upper part of the slope.

3. Wind-tunnel experiments

The Atmospheric Boundary Layer Wind Tunnel Facility located at the University of California, Davis, was used in the present study. A topographic model was constructed from the topographical contour maps that were generated in the field from a survey of the dunes with an electronic theodolite. From the cross sections given in the topographical maps the wind-tunnel models (Fig. 5) were constructed at a scale of 1:154 (Fig. 5). Extensive wind profile measurements have been made for both models. Fig. 6 displays a typical series of mean velocity profiles along the climbing dune surface acquired in the UC Davis wind tunnel. There appears to be reasonable correlation between the scaled up wind tunnel results and those predicted from the FAA model (described in detail in next section), except for one point (shown in Fig. 6a) at heights above 2 m. The wind tunnel results predict greater mean wind speeds above two meters height. However, the critical region in this comparison of wind-tunnel profiles to FAA profiles is ground level. This is the region where particle motion occurs and where it is important to have a good empirical model, such as the FAA model, to use in the solution of particle trajectories. As may be observed from Fig. 6, most of the profiles in the lower two meters have reasonable comparisons between the wind tunnel measurements and the FAA empirical predictions. Consequently, the FAA model was used in the numerical solutions because of this feature and the fact it can be empirically calculated for any position on the escarpment.

Fig. 5. Photograph of climbing dune wind-tunnel model.

4. Numerical solutions of particle motion

The United States Federal Aviation Administration (FAA) complex terrain model for a two-dimensional escarpment was used to provide an analytical model of the changing surface elevation of the climbing dune as a function of position along its surface. Two supporting ideas justify the use of this model. The first reason was the remarkable comparison between the wind-tunnel velocity profiles and those predicted from the FAA model. The second reason was that the velocity profiles and the shape of the escarpment could be analytically described with equations suitable for computer generated numerical solutions.

4.1. Velocity profiles

A one-dimensional flow situation and two-dimensional escarpment model were assumed in which the velocity in the normal direction to the local surface was zero and the velocity u_a in the flow (x) direction (i.e., locally parallel to the surface) was a function of normal distance away from the surface only. The flow geometry and a typical velocity profile are shown on Fig. 7.

In the absence of continuous saltation (i.e., for friction velocities at, just above, or just below the threshold shear velocity), for fully turbulent flow the boundary layer will have a logarithmic velocity profile given by

$$\frac{U_a}{U_*} = \frac{1}{k}\ln\left(\frac{Z}{Z_0}\right) \tag{1}$$

where U_* is the shear velocity, Z_0 the roughness height and k von Karman's constant. For a surface of like particles the roughness height may be taken equal to $1/30Dp$ (Dp is the particle diameter), and with von Karman's constant as 0.4, this equation becomes

$$\frac{U_a}{U_*} = 2.5\ln\left(\frac{Z}{D_p}\right) + 8.5 \tag{2}$$

This profile was assumed to be the undistributed one that would ordinarily exist on a flat horizontal surface. The geometry of the FAA escarpment model is illustrated in Fig. 8 and is mathematically described by

$$e = \frac{h}{1 + \left(\frac{x}{L}\right)^2} \quad \text{for } x < 0 \tag{3}$$

where e is the vertical height, due to the presence of escarpment, above the horizontal plane, i.e., the physical height of the local surface above the undisturbed flat ground; h is the total vertical height of the escarpment, x is the horizontal distance with a zero value location directly beneath the crest of the escarpment as illustrated in Fig. 8; and L is the so-called half horizontal length of the escarpment as measured from the edge of the escarpment to the position where the local surface height decreases to a value of one-half the overall escarpment height, h.

The FAA model uses an approach velocity that is designated by $u_a(z)$, which, in the present case, is given by Eq. (2) above. Here z is always the height above the local ground surface. Local velocities at other locations are designated by $u(x,z)$. At other locations on the escarpments the velocity profile will be altered due to the presence of the escarpment. To account for this effect the following procedure was numerically used in the solution of particle trajectories over the escarpment surface. First, a 'velocity perturbation' factor was defined as

$$\Delta u(x,z) = u(x,z) - u_a(z) \tag{4}$$

and the 'fractional speed-up ratio' was defined as

$$\Delta S = \frac{\Delta u(x,z)}{u_a(z)} \tag{5}$$

Then the 'amplification factor,' A, was given as

$$A = \frac{u(x,z)}{u_a(z)} = 1 + \Delta S(z) \tag{6}$$

The velocity field was then determined by the exact geometry of the escarpment shape for the velocity profiles upwind and over the escarpment up to its crest. Additionally, the maximum wind speed-up factor at the crest was set by the FAA technique which specifies the following guidelines

$$\Delta S_{\max} = 0.8h/L \tag{7}$$

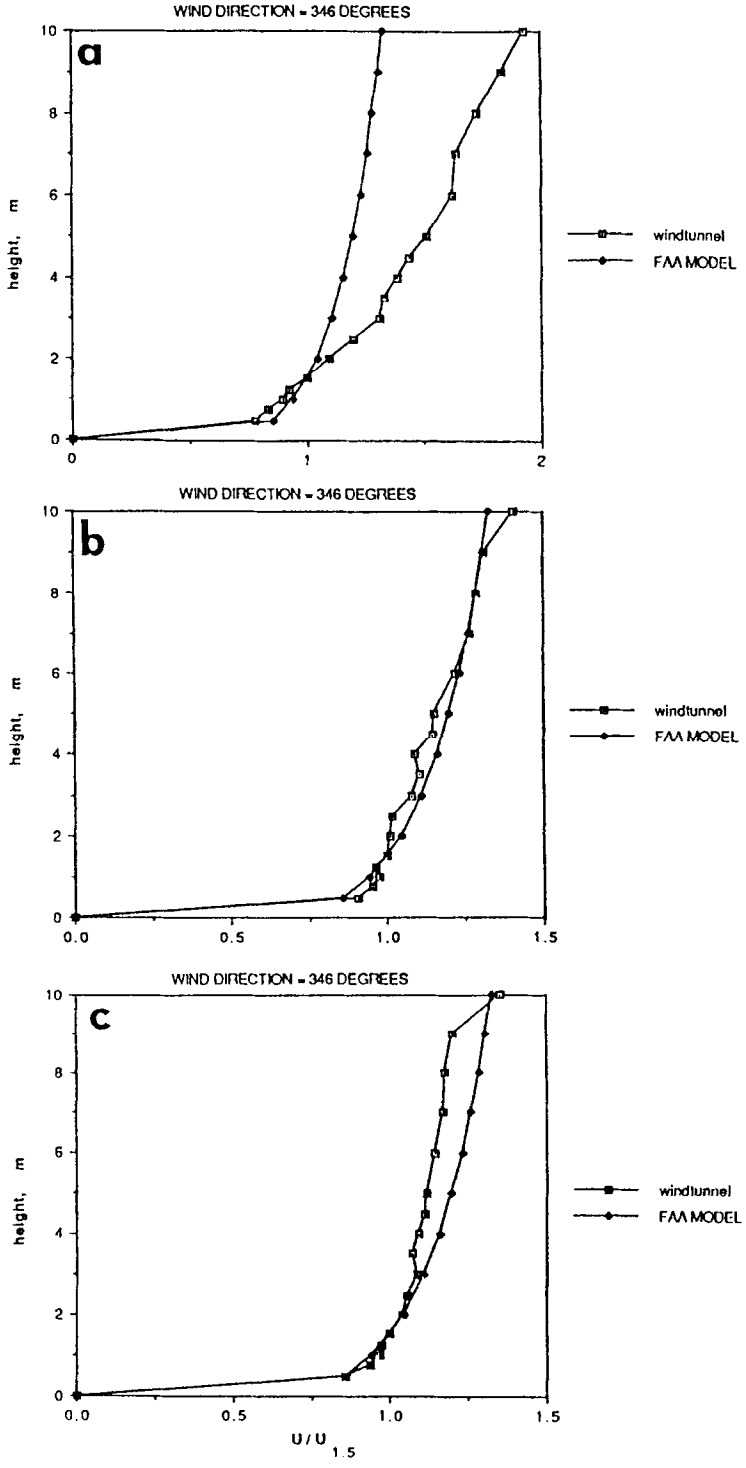
WIND DIRECTION = 346 DEGREES
a
height, m
windtunnel
FAA MODEL
WIND DIRECTION = 346 DEGREES
b
height, m
windtunnel
FAA MODEL
WIND DIRECTION = 346 DEGREES
c
height, m
windtunnel
FAA MODEL
U / U 1.5

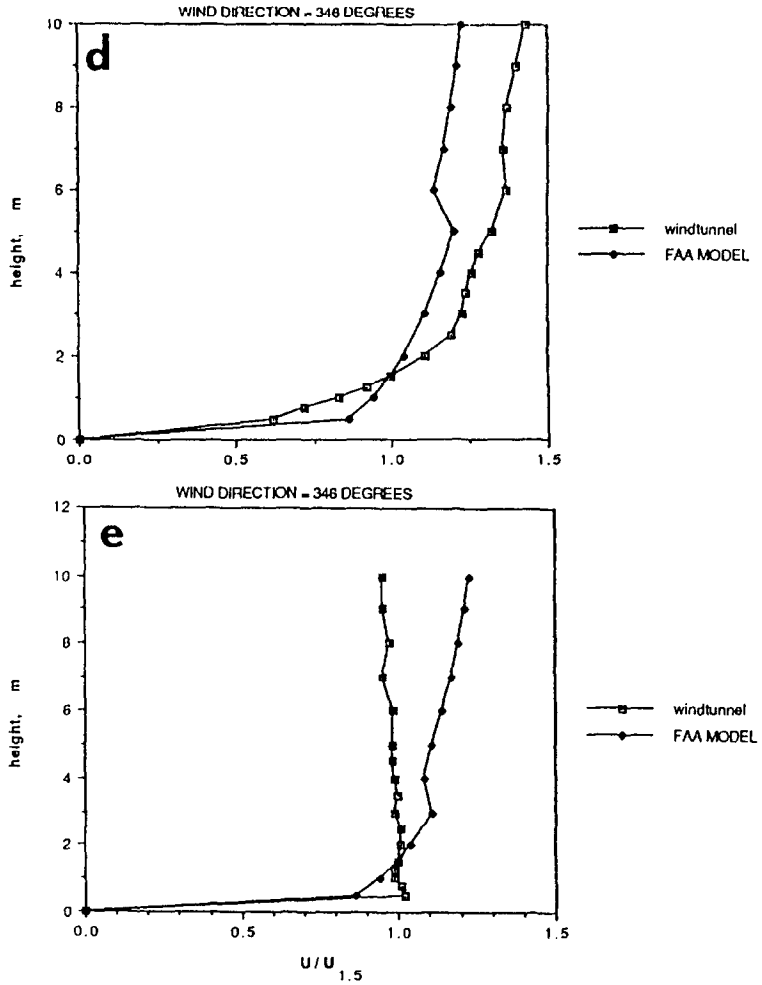

Fig. 6. Normalised velocity as a function of full-scale height for scaled wind-tunnel data and FAA profile calculations at five locations: a) at 20 m upwind of the base of the escarpment; b) at the base of the escarpment; c) at 22 m downwind of the base of the escarpment; d) at 45 m downwind of the base of the escarpment; e) at the escarpment crest.

for two-dimensional escarpments. At heights above the crest or escarpment surface for $x > 0$, the exponential decay law given as

$$\Delta S(o,z) = \Delta S_{\max} \exp[-Ez/L] \quad (8)$$

was used, where $E = 2.5$ for two-dimensional escarpments.

The FAA amplification factors (A) for two-dimensional escarpments, which were used in the above equations for the present work, are presented in Fig. 9. To account for the curve escarpment surface, (i.e., Eq. (3), with usage of the amplification factors displayed in Fig. 9), it was assumed that $A(o,x)$ of the linear escarpment of Fig. 9 was the same as $A(o,x)$ of parabolic escarpment surface of given by Fig. 8 (Eq. (3)).

The above mathematical descriptions completely specifies both the complex surface geometry of the escarpment as well as the analytical flowfield above it, accounting for wind speed-up due to the complex escarpment shape.

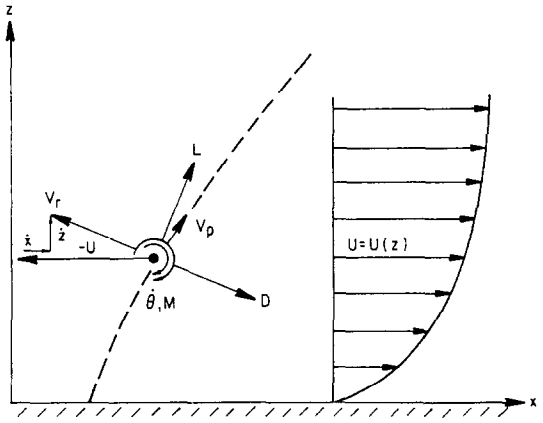

Fig. 7. Local co-ordinate system $z - x$ showing a particle and its trajectory (dashed line) with velocity profile $U_a(z)$. L is particle lift, D is particle drag, V_p is particle velocity, M is particle's moment θ, is particle's spin rate and V_r is the particle relative velocity.

4.2. Equations of motion

The forces acting on a saltating particle tending to change its state of motion are a downward force due to its weight and aerodynamic forces produced by the fluid flowing past it. The latter can be resolved into an equivalent lift force L, drag force D and moment M, as shown in Fig. 7. The direction of the drag force is opposite to the direction of v_r, the velocity of the particle relative to the flow.The equations of motion of a particle can be written as

$$m_p \ddot{x} = L\frac{\dot{z}}{V_r} - D\frac{\dot{x}-u}{Vr} - m_p g \sin\theta \qquad (9)$$

$$m_p \ddot{z} = -L\frac{\dot{x}-u}{V_r} - D\frac{\dot{z}}{V_r} - m_p g \cos\theta \qquad (10)$$

where m_p is the particle's mass, and $\dot{x},\dot{z}$ and $\ddot{x},\ddot{z}$ are the particle's velocity and acceleration components, respectively.

The magnitude of the relative velocity can be expressed in terms of the particle and flow velocities as

$$V_r = \left[(\dot{x}-u)^2 + \dot{z}^2\right]^{\frac{1}{2}} \qquad (11)$$

It has generally been assumed by previous researchers that the drag is the primary fluid force acting on a saltating particle away from the surface and that the lift is very important at very small heights where the influence of the surface becomes important. The effects of lift and drag are customarily expressed in terms of the lift and drag coefficients C_D and C_L defined by

$$L = \frac{1}{2}C_L A_p \rho V_r^2;\ D = \frac{1}{2}C_D A_p \rho V_r^2 \qquad (12)$$

where A_p is the particle's cross-sectional area.

If the particles are assumed spherical and of uniform density, then the equations of motion including both lift and drag forces simplify to

$$\ddot{x} = -\frac{3\rho V_r}{4\rho_p D_p}\left[C_D(\dot{x}-u) - C_L\dot{z}\right] - g\sin\theta \qquad (13)$$

$$\ddot{z} = \frac{3\rho V_r}{4\rho_p D_p}\left[C_D\dot{z} - C_L(\dot{x}-u)\right] - g\cos\theta \qquad (14)$$

4.3. Lift and drag coefficients

The initial conditions are same as those used by White et al. (1976). Initially, the particle is at rest on the surface, and as the wind speed is increased above threshold, particles begin to move. The expressions for the lift coefficients are presented by (White et al., 1976). The drag coefficient of a sphere is strongly dependent on the Reynolds number. A number of empirical representations for this dependence have been developed. Perhaps the best of these is given in the paper by Morsi and Alexander (1972), who derived a set of equations expressing the relationships between the drag coefficient and Reynolds

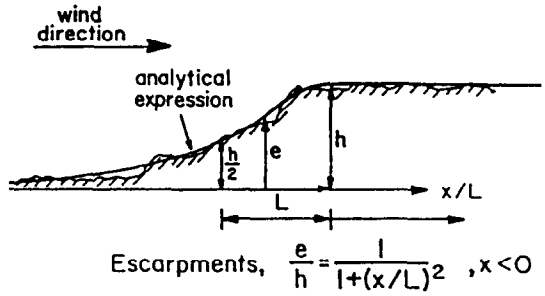

Fig. 8. FAA analytical description of two-dimensional escarpment shape.

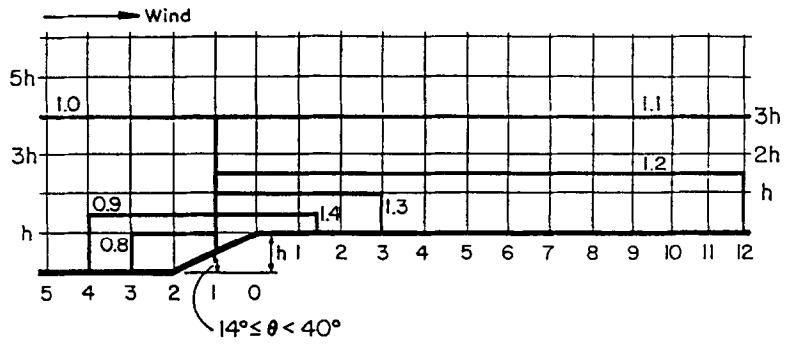

Fig. 9. Schematic diagram displaying the values of the amplification factors, A, for various positions around and over the two-dimensional escarpment shapes.

number over the entire Reynolds number range. Their equations were used to calculate the drag coefficients needed in the numerical integrations performed in the present research.

4.4. Results of solutions

The height of the escarpment at its crest was set at 20 m and the length was determined, from the electronic theodolite field contour map, to be 53 m (assuming an average escarpment angle of about 22 degrees as measured both in the field and from the electronic theodolite map). The undisturbed value of shear velocity was set at 30 cm s^{-1} and the trajectories of three sized particles (0.130, 0.230 and 0.330 mm; or 2.94, 2.12 and 1.60 ϕ values, respectively) were calculated for seven positions along the escarpment surface. The location of the trajectory length calculation is given in X/L where X is the distance of the point from the crest of the dune and L is the entire length of the dune slope: (1) the upwind undisturbed wind profile which was placed at 47 m upwind of the dune plinth ($X/L = -1.90$); (2) $X/L = -1.40$; (3) $X/L = -1.00$ (the base of the escarpment); (4) $X/L = -0.58$; (5) $X/L = -0.15$; (6) $X/L = 0$ (at the escarpment crest); and, (7) $X/L = 0.38$. The results of the particle trajectories pathlengths (L) are presented in Fig. 10, Figs. 11 and 12.

Key results from the trajectory calculations are that the 0.330 mm sized particles are stopped at the base of the climbing dune and that those sized particles already present would be only moved in the upper elevations of the surface. The result, for this commonly occurring shear velocity, would be that the supply of 0.330 mm (1.60ϕ) sized particles soon would be depleted from the upper half of the dune since no new particles of the same size would be

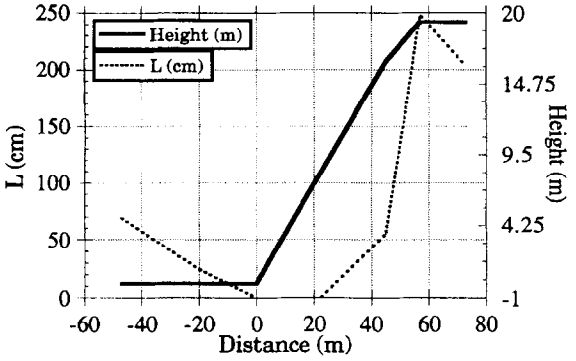

Fig. 10. Trajectory pathlength (L), along the slope of the climbing dune (shown in cross section), for saltating grain sized 0.33 mm.

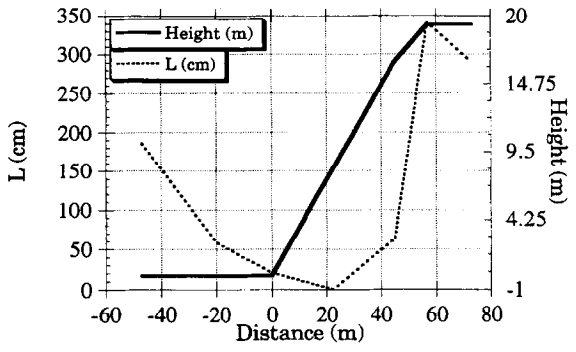

Fig. 11. Trajectory pathlength (L), along the slope of the climbing dune (shown in cross section), for saltating grain sized 0.23 mm.

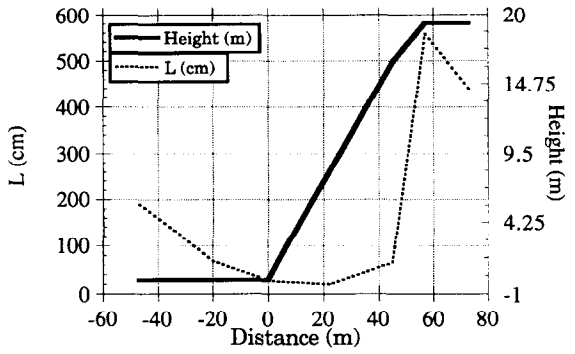

Fig. 12. Trajectory pathlength (L), along the slope of the climbing dune (shown in cross section), for saltating grain sized 0.13 mm.

moving upwards. This feature was observed in the size distribution analysis taken in the field samples (Fig. 4). Also, the 0.230 mm (2.12ϕ) particles would be stopped in the lower one-third height region of the dune due to diminished surface stress insufficient to move them. This feature also is consistent with the results of the field samples taken in this location on the dune (i.e., no further movement of 0.230 mm particles and coarser to higher positions on the escarpment as shown by Figs. 3 and 4).

It is presumed that bimodality of the grain size distribution is the outcome of the diminution of the trajectories of the grains coarser than 0.177 mm ($< 2.50\phi$) at the lower one-third height region of the dune. Only sand samples that were retrieved from the lower half of the dune show bimodality (Samples 2, 2–3, and 3 in Fig. 4) while the distribution of the grain size in the upper part of the slope (Samples 3–4, and 4) is unimodal as a result of considerable decreasing of grains coarser than 0.177 mm.

All traps at Points 2 and 2–3 show a considerable deficiency in the range of 0.177–0.250 mm ($2–2.5\phi$) relative to the sand retrieved from the surface (Figs. 3 and 4). The missing range probably consists of grains that are mostly transported by surface creep. The trap used in the field work can only collect grains in saltation.

Particle trajectories at the crest of the dune and further downwind ($X/L > 0$) display extra-long pathlengths ranging from two to three times their respective undisturbed pathlengths. Again this feature is consistent with field observation, with the exception of the formulation of a cliff-top dune at the crest of the slope. This dune was caused by a flow separation and a resulting recirculation region occurring just downwind of the crest area on the escarpment. This feature of the field flow was not modelled.

5. Conclusions

1. All particle motion (pathlengths) are diminished at the base of the climbing dune as well as just upwind and downwind of the base area of the escarpment.
2. Particles coarser than 0.250 mm ($< 2\phi$) are unable to reach the crest of the dune for a shear velocity of 30 cm s^{-1}.
3. Particles in the range 0.177–0.350 mm (1.5–2.5ϕ) cease their movement at lower half of the climbing dune and therefore tend to accumulate there. Because of deficiency of this range in the traps it is presumed that they mostly move by surface creep and not saltation.
4. Particles smaller than 0.177 mm ($> 2.5\phi$) are transported in the saltation mode. These particles, which consist about 90% of the particles in the traps, climbed the dune's slope when the undisturbed wind shear velocity was between 13 and 18 cm s^{-1}.

Acknowledgements

The authors wish to thank Alon Guvrin for analysing the field data, and Elad Taig and Etoli Wolff for the computer work. This research was supported by grant No 90-00253 from the United States — Israel Binational Science Foundation (BSF), Jerusalem, Israel.

References

Ahlbrandt, T.S., 1979. Textural parameters of aeolian deposits. In E.D. McKee (Editor), A study of global sand seas. United States Geological Survey, Professional Paper, Washington, pp. 21-51.

Anderson, R.S., 1989. Saltation of sand: a qualitative review with biological analogy. Proc. Roy. Soc. Edin., 96B: 149-165.

Anderson, R.S., Sørensen, M. and Willetts, B.B., 1991. A review of recent progress in our understanding of aeolian sediment transport. Acta Mech. (Suppl.), 1: 1-19.

Bagnold, R.A., 1941. The physics of blown sand and desert dunes. Methuen, London.

Chepil, W.S., 1945. Dynamics of wind erosion: I. Nature of movement of soil by wind. Soil Sci., 60: 305-320.

Hunt, J.C.R., Leibovich, S. and Richards, K.J., 1988a. Turbulent shear flow over low hills. Quart. J. Roy. Meteorol. Soc., 114: 1435-1470.

Hunt, J.C.R., Richards, K.J. and Brighton, P.W.M., 1988b. Stratified shear flow over low hills. Quart. J. Roy. Meteorol. Soc., 114: 859-886.

Jackson, P.S. and Hunt, J.C.R., 1975. Wind flow over a low hill. Quart. J. Roy. Meteorol. Soc., 101: 929-955.

Jensen, N.O. and Zeman, O., 1985. Perturbation in mean wind and turbulence in flow over topographic forms. Proc. of the Int. Workshop of the Physics of Blown sand, Dept. Theoretical Statistics, Inst. of Mathematics, Univ. Aarhus, Memoir No. 8, pp. 351-368

Leatherman, S.P., 1978. A new aeolian sand trap design. Sedimentol., 25: 303-306.

Morsi, S.A. and Alexander, A.J., 1972. An investigation of particle trajectories in two-phase flow systems. J. Fluid Mech., 55: 193-208.

Nielson, J. and Kocurek, G., 1986. Climbing zibars of the Algodones. Sed. Geol., 48: 1-15.

Pye, K. and Tsoar, H., 1990. Aeolian Sand and Sand Dunes. Unwin Hyman, London.

Taylor, P.A. and Gent, P.R., 1974. A model of atmospheric boundary layer flow above an isolated two-dimensional hill; an example of flow above gentle topography. Boundary-Layer Meteorol., 7: 349-362.

Tsoar, H., 1986. Two-dimensional analysis of dune profile and the effect of grain size on sand dune morphology. In F. El-Baz and M.H.A. Hassan (Editors), Physics of desertification. Martinus Nijhoff, Dordrecht, pp. 94-108.

Tsoar, H., 1990. Grain size characteristics of wind ripples on a desert seif dune. Geography Research Forum, 10: 37-50.

White, B.R., Greeley, R.G., Iversen, J.D. and Pollack, J.B., 1976. Estimated grain saltation in a Martian atmosphere. J. Geophys. Res., 81: 5643-5650.

Willetts, B.B. and Rice, A., 1989. Collisions of quartz grains with a sand bed: the influence of incident angle. Earth Surf. Processes and Landforms, 14: 719-730.